Tailored Nanoheterojunctions for Optimized Light Emission

Tianshu Li, Francois Gygi, and Giulia Galli

Phys. Rev. Lett. **107**, 206805 — Published 8 November 2011

DOI: 10.1103/PhysRevLett.107.206805

Tailored nanoheterojunctions for optimized light emission

Tianshu Li,[1,*] Francois Gygi,[2,3] and Giulia Galli[4,5]

[1]*Department of Civil and Enviromental Engineering, George Washington University, Washington, DC 20052*

[2]*Department of Applied Science, University of California, Davis, CA 95616, USA*

[3]*Department of Computer Science, University of California, Davis, CA 95616, USA*

[4]*Department of Chemistry, University of California, Davis, CA 95616*

[5]*Department of Physics, University of California, Davis, CA 95616, USA*

Abstract

We present coupled classical and quantum simulations of 1 to 2 nm Si nanocrystals (NCs) embedded in amorphous SiO_2 and we show that by tuning the density of the oxide matrix, one may change the relative alignment of Si NC and SiO_2 electronic states at the interface. We find that interfacial strain plays a key role in determining the variation of the nanaoparticle gap as a function of size, as well as of conduction band offsets with the oxide. In particular, our results show that it is the variation of the valence band offset with size that is responsible for the gap change. Our findings suggest that the elastic properties of the embedding matrix may be tuned to tailor the energy levels of small Si NCs so as to optimize their performance in opto-electronic devices and solar cells.

The discovery of light emission from Si-NCs embedded in amorphous matrices [1] holds great promises for extending Si technology to opto-electronic circuits [2]. The versatility of light-emitting matrix-based systems may provide alternative routes towards the fabrication of optically active CMOS-devices, and it constitutes an active field of research. However to understand and eventually control photoluminescence and absorption properties of Si-NCs, important ingredients are still missing, including the microscopic characterization of the interface between the nanoparticle and the matrix. Such a characterization is equally important to unravel possible charge traps when using NCs for solar cells and to elucidate energy transfer processes when NCs are implanted, *e.g.*, with lanthanide ions.

Robust experimental techniques to probe nano-interfaces at the microscopic level are not yet available, although valuable progress has been reported in recent years [3, 4]. In addition, experimentally it remains difficult to identify the electronic states contributing to measured photoluminescence spectra. Most theoretical studies have focused on isolated nanoparticles [5–7] where interfacial effects have been simply modeled by adding *ad hoc* surfactants to the nanoparticle surface, with the exception of recent structural studies using, *e.g.*, network switching algorithms [8–11]. In fact, devising a microscopic model of embedded NCs is rather challenging due to the lack of structural data from experiment and to the difficulty of treating explicitly an amorphous matrix in electronic structure calculations. Therefore models of nanoparticles in realistic environments, and thus directly comparable with experiment, are largely unavailable. In particular, a study of Si nanocrystals embedded in amorphous SiO_2, including the identification of the overall matrix effect on the properties of the nanoparticles, has not yet been carried out.

Here we report an investigation of Si nanocrystals in an amorphous SiO_2 matrix conducted by combining classical molecular dynamics (MD) and quantum simulations based on Density Functional Theory (DFT). Our results show that both interfacial strain and the matrix density play a key role in determining the opto-electronics properties of the nanocrystals, which cannot be described using simple quantum confinement models. Our findings also points at ways of tuning the alignment of nanocrystals and the oxide's electronic states by controlling the matrix elastic properties so as to optimize the NCs performance in opto-electronic devices and in solar cells.

In order to build a realistic atomistic model of the silicon dioxide matrix, we started from a β-cristobalite cell containing 1536 atoms which was compressed so as to match its Si sub-

lattice with that of crystalline Si. We then removed all oxygen atoms from a given spherical region of diameter d. This configuration was used as the starting geometry of annealing cycles aimed at amorphizing the SiO_2 matrix. The density (ρ) of the composite system was first chosen based on a simple rule of mixing, using the equilibrium, experimental density of amorphous SiO_2 and crystalline Si. We call this density ρ_0. At a later stage ρ was modified to investigate explicitly the effect of the matrix density on the nanocrystals' properties. Annealing cycles were carried out using classical MD simulations and employing an *ab initio* derived augmented Tersoff potential [12–14]. During the relatively slow annealing process (duration $>$ 15 ns), the Si nanocrystal's atomic positions were kept fixed up to 750 K, below which all atoms were allowed to move. We first describe the composite system at density ρ_0.

The annealed composite structure contains Si-O-Si bridge bonds at the NC/matrix interface. This is not unexpected as Si-O-Si bonds are the dominant ones in the amorphous SiO_2. A few hydrogen atoms were added to the system in order to passivate unsaturated bonds in the matrix. The composite structure obtained in this way was further optimized by performing *ab initio* MD simulations with the QBOX code [15] using the Perdew-Burke-Ernzerhof functional [16], and norm-conserving pseudopotentials with an energy cut-off of 60 Ry. To cross-check our results, we also repeated our electronic structure calculations for the 1.5 nm Si NC by employing the Perdew-Zunger functional [17] (see Table 1). Three diameters: 1.3 nm, 1.5 nm, and 1.9 nm, were chosen, corresponding to nanocrystals with 61, 102, and 217 Si atoms (model #1 $\sim$ 3) respectively. The smallest Si nanocrystal (d = 1.3 nm) was also investigated using a β-cristobalite cell containing 648 atoms, following the same procedure as described above, in order to study possible size effects in our calculations (model #4). Size effect were found to be negligible. A summary of the properties of the composite NC/matrix systems obtained in our simulations at density ρ_0 is given in Table 1.

Figure 1 (a) shows the calculated electronic density of states (EDOS) of Si nanocrystals embedded in amorphous SiO_2 matrices with density ρ_0. The electronic structure analysis was carried out using the QUANTUM ESPRESSO code [18]. As a comparison, the EDOS of an amorphous SiO_2 sample containing 216 atoms and generated using the same inter-atomic potential is also included. The computed electronic gap of a-SiO_2 is about 5.4 eV, smaller than the experimental value of 9 eV [19]; this underestimate is typical of DFT calculations using local and semi-local functionals, and it is consistent with previous predictions [20, 21]

based on *ab initio* MD simulations. The matrix with density ρ_0 and the nanoparticles form a nano heterojunction of so called type I, with straddling gaps, that is the energy gap of the Si nanoparticle falls within the gap of the oxide. As a result, the composite structure exhibits a much smaller energy gap than that of a-SiO_2; this gap increases from 1.43 eV to 1.76 eV as the size of the Si nanocrystal decreases from 1.9 nm to 1.3 nm. A similar trend in the variation of the gap with size has been found both in experiments [22–25] and in first principle computations of hydrogenated free-standing Si nanocrystals [5, 7, 26], and it has been generally attributed to the combined effects of quantum confinement and oxygen related surface defects. In particular, in free standing Si and Ge nanocrystals, experiments showed that both the VB and CB edges shift with the size of the nanocrystal, resulting in an increased band gap for smaller particles [27, 28].

In the embedded system, we find that the origin of the gap change as a function of size is much more complex. The inset of Fig.1 (a) shows that as the size of the Si NC decreases, the VB edge shifts to a lower energy, while the position of the CB edge is hardly affected, yielding an overall increase of the energy gap. This finding is in excellent agreement with the soft x-ray spectroscopy measurements of the band edges of embedded Si NCs of sizes as small as 1.6 nm [29]. To understand this behavior, we analyzed the spatial distribution of the wavefunctions of the VB and CB edges. Fig. 1 (b) and (c) show the charge density iso-surfaces of the highest occupied molecular orbitals (HOMO) and the lowest unoccupied molecular orbitals (LUMO) of the Si NC/a-SiO_2 composite, respectively, for $d = 1.9$ nm. As in all models studied here, the electronic states in the vicinity of the energy gap are mostly localized on the nanoparticle, but the charge density distributions associated with the HOMO and LUMO are substantially different. The LUMO is extended over the entire nanocrystal, while the HOMO is mostly localized in the interfacial region between the nanoparticle and the surrounding matrix. Such HOMO and LUMO charge distributions differ from those found for hydrogenated free-standing Si nanoclusters with both unreconstructed and reconstructed surfaces [6], where a clear distinction between localization of HOMO and LUMO could not be identified.

These results point at a significant role played by the matrix on the localization of the HOMO state. To understand the effect, we analyzed the strain induced on the nanoparticle by the oxide. We note that the local normal strain, *i.e.*, the variation of the nearest Si-Si bond length with respect to those in the bulk Si, is not a good indicator of the local

strain field: At the same radius from the center of the Si NC, the normal strain may be found to be either tensile or compressive locally, and the average normal strain almost vanishes. Instead, we analyzed the distortions induced on the nanoparticle by the oxide, in the interfacial region. In particular, the presence of bridging O atoms causes significant distortions of the Si lattice near the surface of the nanocrystal. We analyzed interfacial distortions by employing a local order parameter q_3 [30], a quantity that is highly sensitive to tetrahedral order. The radial distributions of q_3 parameters for three Si NCs are shown in Fig. 2, where two general trends are revealed. First, the overall tetrahedrality decreases with the size of the nanocrystal. Second, for a given nanoparticle, the bonding configurations are more disordered at the surface than in the core.

It is interesting to understand whether the matrix influence observed in our calculations is exerted primarily through the induced strain at the surface, or whether the overall electronic structure of the NC is affected due to the lack of separation between matrix and NC's electronic states. To address this question, we compared the electronic structures of embedded and free-standing nanocrystals inclusive of an interfacial oxide layer shell. We call the latter coated NC. To define an appropriately coated nanoparticle, we extracted the Si cores from the composite structure and we included the atoms belonging to the first nearest neighbors of the outermost Si atoms; we then passivated the surface dangling bonds with H atoms. The resulting structures were relaxed *ab initio* to the nearest local energy minimum. Structural optimization (see Fig. 3 a and c) has a negligible effect on the geometry, and only the surface H atoms undergo significant relaxations. The spatial distribution of HOMO-LUMO orbitals of the coated nanoparticle of diameter 1.5 nm is shown in Fig. 3. Similar to the case of the embedded nanocrystal (Fig. 3a), the HOMO is found to be localized at the surface (mostly on Si atoms) and the LUMO is extended over the entire particle. The HOMO-LUMO gap (1.63 eV) of the coated and embedded NCs are identical. Therefore, although the role played by the matrix is very important (as it determines the character of the HOMO and LUMO states), the effect of the matrix appears to be fairly localized and limited to the first layer oxide in direct contact with the NC. To further confirm this interpretation, we compared the site-projected density of states (PDOS) of the coated and embedded NCs. Fig. 3 b and d show that the PDOSs of the two systems are virtually identical. The same behavior was also found for the other two models generated in our simulations. These results confirm that the major role induced by the amorphous matrix is a strain-induced geometry change

at the surface.

It is interesting to analyze whether changes in the matrix density may lead to substantial changes in the type of interfaces formed between the nanoparticle and the matrix. To this end, we considered a macroscopic density of the matrix larger than ρ_0 by 15%, *i.e.*, $\rho = 1.15\rho_0$ (model #5 in Table 1), and found a qualitative change in the alignment of the energy levels at the interface (see Fig. 4 where we give a schematic representation of our results). In particular the LUMO of the nanocrystal (we considered $d = 1.5$ nm) falls above the CB minimum of the matrix and the gap of the composite system is between the HOMO of the nanoparticle and the CB minimum of the oxide, indicating that the nanoparticle loses its electronic identity in the matrix. In this case the nano heterojunction is of type II and it would be more promising for charge extraction in the case of solar cell applications. Our structure analysis indicates that the increase of matrix density has very little influence on the core structure of the Si NC, as indicated by the calculated q_3 of a 1.5 nm Si NC embedded in the high density matrix, shown in Fig. 3. On the other hand, we also found that the major change accompanying the density increase in the SiO_2 matrix is a decrease of the Si-O-Si bond angle. A previous study [31] has shown that the electronic contribution of the dielectric constant (ϵ_∞) increases as the Si-O-Si bond angle decreases, thus leading to a decrease of the energy band gap of SiO_2 under pressure. Therefore our finding on the variation of the band alignment at interface is consistent with the changes found in the electronic structures of the matrix and the Si NC as the composite becomes denser.

These results show that the macroscopic density of the host matrix may greatly influence the level alignments at the interface. In the case of the high density matrix the gap is not an intrinsic property of the embedded Si nanocrystals. It is conceivable to expect that depending on preparation conditions, the matrix density may not be uniform and thus different types of interfaces may be formed within the same composite, leading, *e.g.*, to dark or bright nanoparticles within the same matrix. In the case of type I interfaces, we have shown that the induced local deformation at the surface plays a key role in determining the localization of the HOMO state and thus hole energy levels and conduction band offsets are strongly affected by the oxide. This may in turn greatly influence charge separation and extraction in the case of solar cell applications. Our findings also indicate that the opto-electronic properties of Si nanocrystals should vary if the chemical composition of the matrix is varied. For example, in Si_3N_4 amorphous matrices [32], N tends to bind to three

neighbor Si atoms in a nearly planar configuration. Furthermore, both experiment [33] and theoretical predictions [21, 34] have revealed that two-fold coordinated N atoms, *i.e.*, Si-N-Si bond angles of about 90^o, are present in amorphous Si_3N_4. Thus the induced local deformation due to the bridging N atom is expected to be rather different from that induced by Si-O-Si bridges, and this will influence the HOMO position, and the localization of hole states. Finally our results point at ways of engineering specific interfaces with nanocrystals and thus at devising specific energy gaps and electronic properties by controlling the elastic properties of the surrounding matrix.

The authors thank D.Donadio and L. Dal Negro for discussion. This work was supported by DOE/BES (contract number DE-FG02-06ER46262) and DOE/SciDAC (contract number DE-FC02-06ER25794).

* corresponding author:tsli@gwu.edu

[1] L. Pavesi, L. D. Negro, C. Mazzoleni, G. Franzo, and F. Priolo, Nature **408**, 440 (2000).

[2] L. Canham, Nature **408**, 411 (2000).

[3] S. Godefroo, M. Hayne, M. Jivanescu, A. Stesmans, M. Zacharias, O. I. Lebedev, G. V. Tendeloo, and V. V. Moshchalkov, Nature Nanotech **3**, 174 (2008).

[4] D. M. Aruguete, M. A. Marcus, L.-S. Li, A. Williamson, S. Fakra, F. Gygi, G. A. Galli, and A. P. Alivisatos, J Phys Chem C **111**, 75 (2007).

[5] A. Puzder, A. Williamson, J. Grossman, and G. Galli, Phys. Rev. Lett. **88**, 097401 (2002).

[6] A. Puzder, A. Williamson, F. Reboredo, and G. Galli, Phys. Rev. Lett. **91**, 157405 (2003).

[7] Z. Zhou, L. Brus, and R. Friesner, Nano Lett **3**, 163 (2003).

[8] G. Hadjisavvas and P. Kelires, Phys. Rev. Lett. **93**, 226104 (2004).

[9] K. Seino, F. Bechstedt, and P. Kroll, Phys. Rev. B **82**, 085320 (2010).

[10] T. Pennycook, G. Hadjisavvas, J. Idrobo, P. Kelires, and S. Pantelides, Phys. Rev. B **82**, 125310 (2010).

[11] R. Guerra, E. Degoli, and S. Ossicini, Phys. Rev. B **80**, 155332 (2009).

[12] S. R. Billeter, A. Curioni, D. Fischer, and W. Andreoni, Phys. Rev. B **73**, 1 (2006).

[13] M. Ippolito, S. Meloni, and L. Colombo, Appl. Phys. Lett. **93**, 153109 (2008).

[14] D. Fischer, A. Curioni, S. Billeter, and W. Andreoni, Appl. Phys. Lett. **88**, 012101 (2006).

[15] F. Gygi, "Qbox, a scalable implementation of first-principles molecular dynamics," http://eslab.ucdavis.edu.

[16] J. Perdew, K. Burke, and M. Ernzerhof, Phys. Rev. Lett. **77**, 3865 (1996).

[17] J. Perdew and A. Zunger, Phys. Rev. B **23**, 5048 (1981).

[18] P. Giannozzi *et al.*, J Phys-Condens Mat **21**, 395502 (2009).

[19] S. Miyazaki, H. Nishimura, M. Fukuda, L. Ley, and J. Ristein, Applied Surface Science **113**, 585 (1997).

[20] J. SARNTHEIN, A. PASQUARELLO, and R. CAR, Phys. Rev. Lett. **74**, 4682 (1995).

[21] L. Giacomazzi and P. Umari, Phys. Rev. B **80**, 144201 (2009).

[22] V. A. Belyakov, V. A. Burdov, R. Lockwood, and A. Meldrum, Advances in Optical Technologies **2008**, 1 (2008).

[23] M. Wolkin, J. Jorne, P. Fauchet, G. Allan, and C. Delerue, Phys. Rev. Lett. **82**, 197 (1999).

[24] G. Ledoux, J. Gong, F. Huisken, O. Guillois, and C. Reynaud, Appl. Phys. Lett. **80**, 4834 (2002).

[25] T. Kim, N. Park, K. Kim, G. Sung, Y. Ok, T. Seong, and C. Choi, Appl. Phys. Lett. **85**, 5355 (2004).

[26] A. Puzder, A. Williamson, J. Grossman, and G. Galli, J. Am. Chem. Soc. **125**, 2786 (2003).

[27] T. van Buuren, L. Dinh, L. Chase, W. Siekhaus, and L. Terminello, Phys. Rev. Lett. **80**, 3803 (1998).

[28] C. Bostedt, T. van Buuren, T. Willey, N. Franco, L. Terminello, C. Heske, and T. Moller, Appl. Phys. Lett. **84**, 4056 (2004).

[29] A. Zimina, S. Eisebitt, W. Eberhardt, J. Heitmann, and M. Zacharias, Appl. Phys. Lett. **88**, 163103 (2006).

[30] T. Li, D. Donadio, L. M. Ghiringhelli, and G. Galli, Nat Mater **8**, 726 (2009).

[31] D. Donadio, M. Bernasconi, and F. Tassone, Phys. Rev. B **68**, 134202 (2003).

[32] L. D. Negro, J. Yi, L. Kimerling, S. Hamel, A. Williamson, and G. Galli, Appl. Phys. Lett. **88**, 183103 (2006).

[33] W. Warren, P. Lenahan, and S. Curry, Phys. Rev. Lett. **65**, 207 (1990).

[34] T. A. Pham, T. Li, S. Shankar, F. Gygi, and G. Galli, Appl. Phys. Lett. **96**, 062902 (2010).

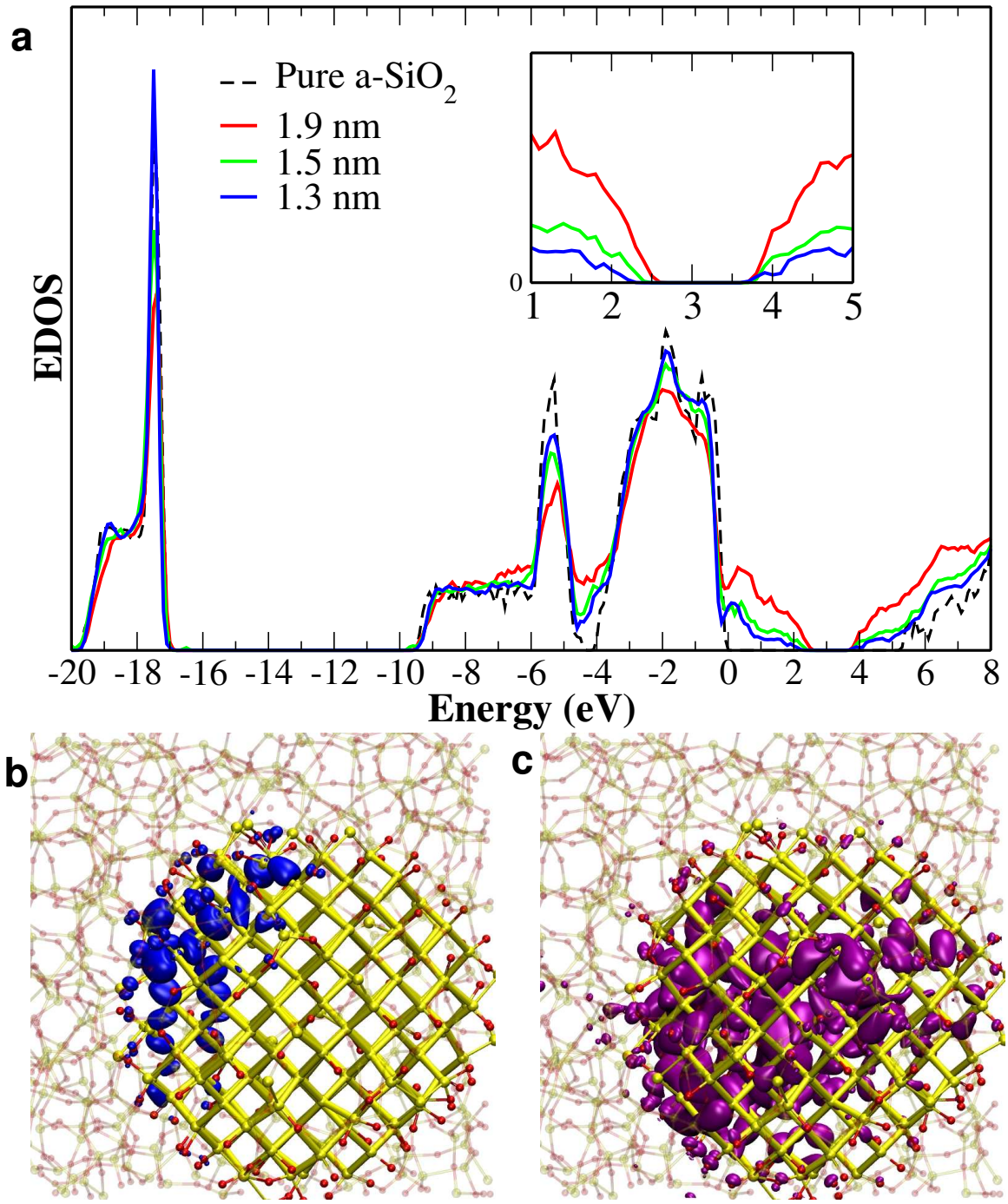

FIG. 1. (**a**) Calculated total electronic density of states (EDOS) of three models (see text). The dashed line indicates the EDOS of pure amorphous SiO_2. The insert shows a zoom-in of EDOS in the vicinity of the band gap. The square moduli of HOMO (blue) and LUMO (purple) of 1.9 nm Si NC embedded in the matrix (The overall chemical formula of such composite is $Si_{512}O_{575}H_{32}$) are shown in (**b**) and (**c**), respectively. The valence band top of pure amorphous SiO_2 is set at zero. The HOMO-LUMO levels are 2.42-3.86 eV, 2.26-3.89 eV, and 2.14-3.90 eV for Si NCs of 1.3 nm, 1.5 nm, and 1.9 nm, respectively.

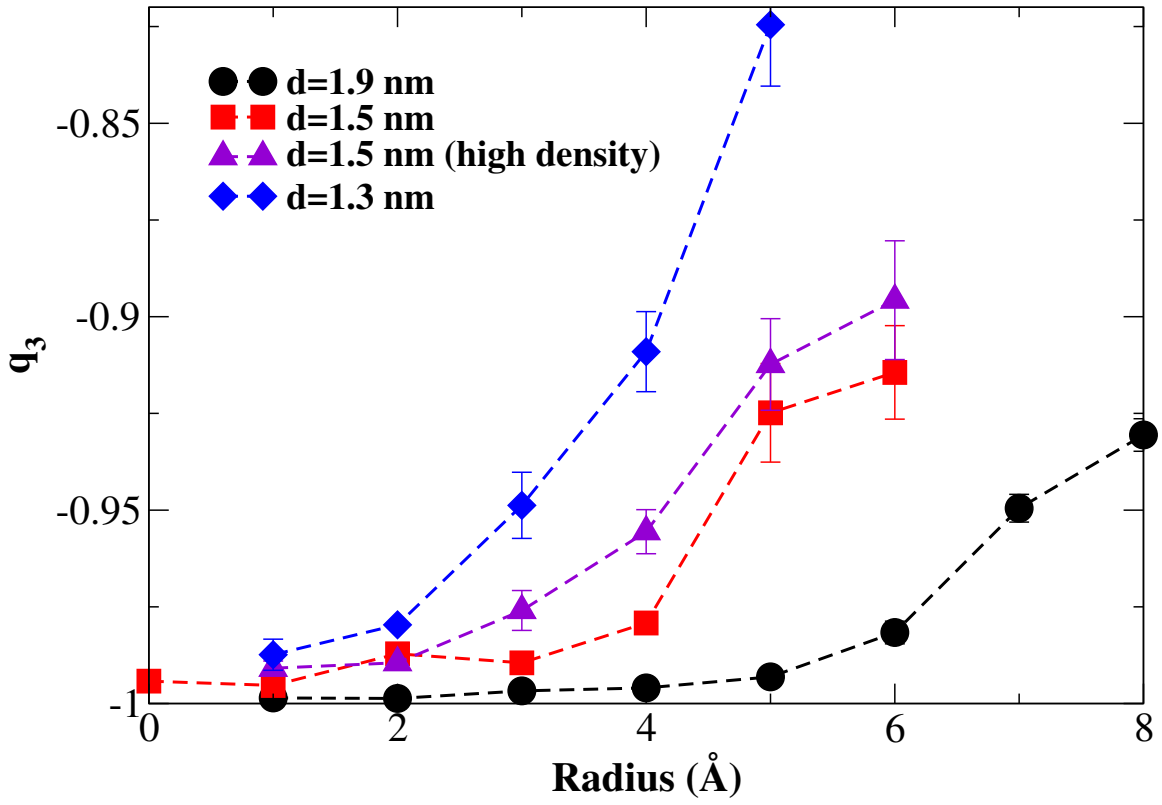

FIG. 2. Radial distribution of the local order parameter q_3 (see text) of embedded Si nanocrystals with different diameters. The value -1 corresponds to the Si atoms in the perfect diamond lattice positions.

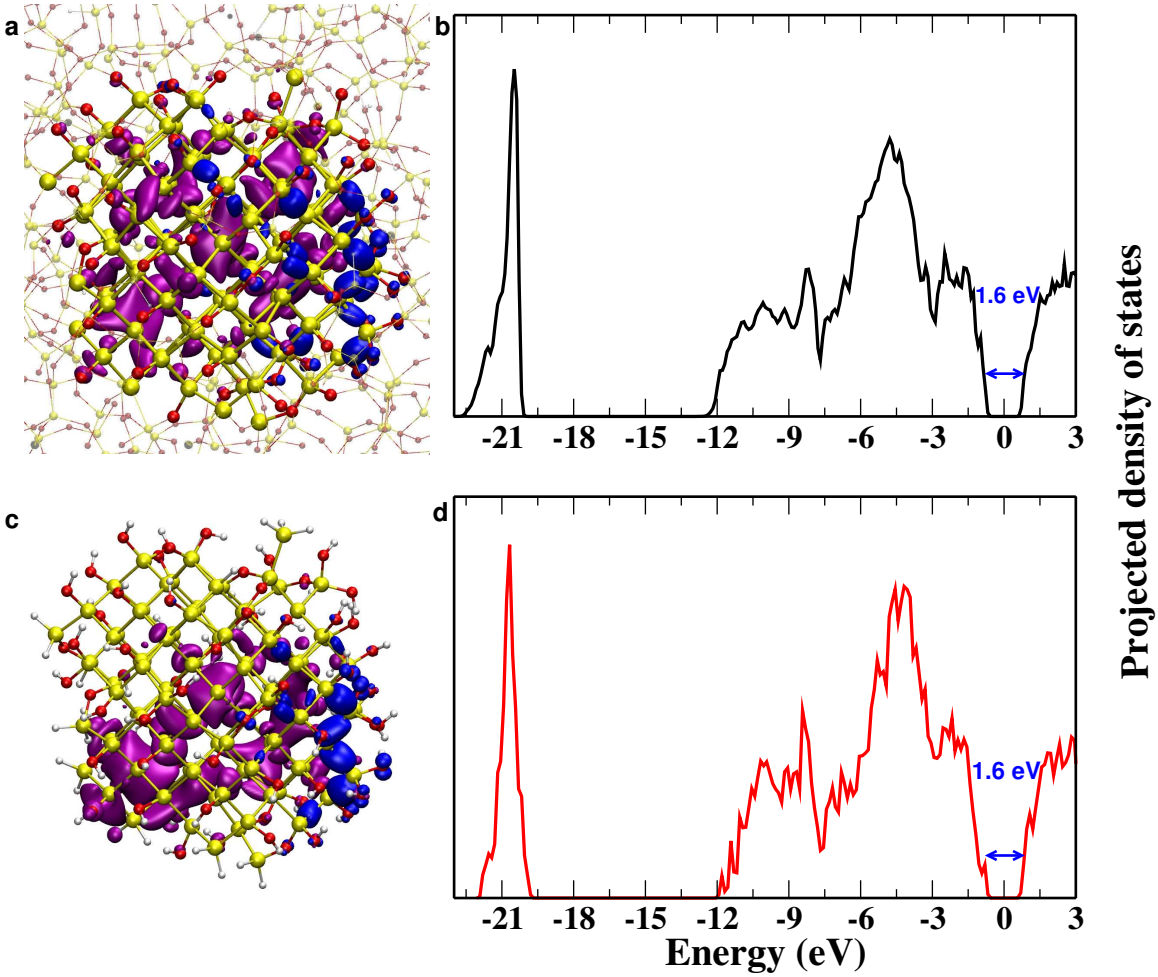

FIG. 3. Distribution of the square moduli of the HOMO (blue) and LUMO (purple) orbitals in (**a**) embedded and (**c**) coated Si nanocrystals. The coated nanoparticle ($Si_{116}O_{72}H_{84}$) is composed by the Si NC and the first oxide shell (see text). The diameter of NC is 1.5 nm (model II in Table 1). The Si and O atoms are shown in yellow and red, respectively. The atomic-site projected density of states (projected onto the Si cores) of the embedded Si nanocrystal (**b**) is almost identical to that of the coated NCs.

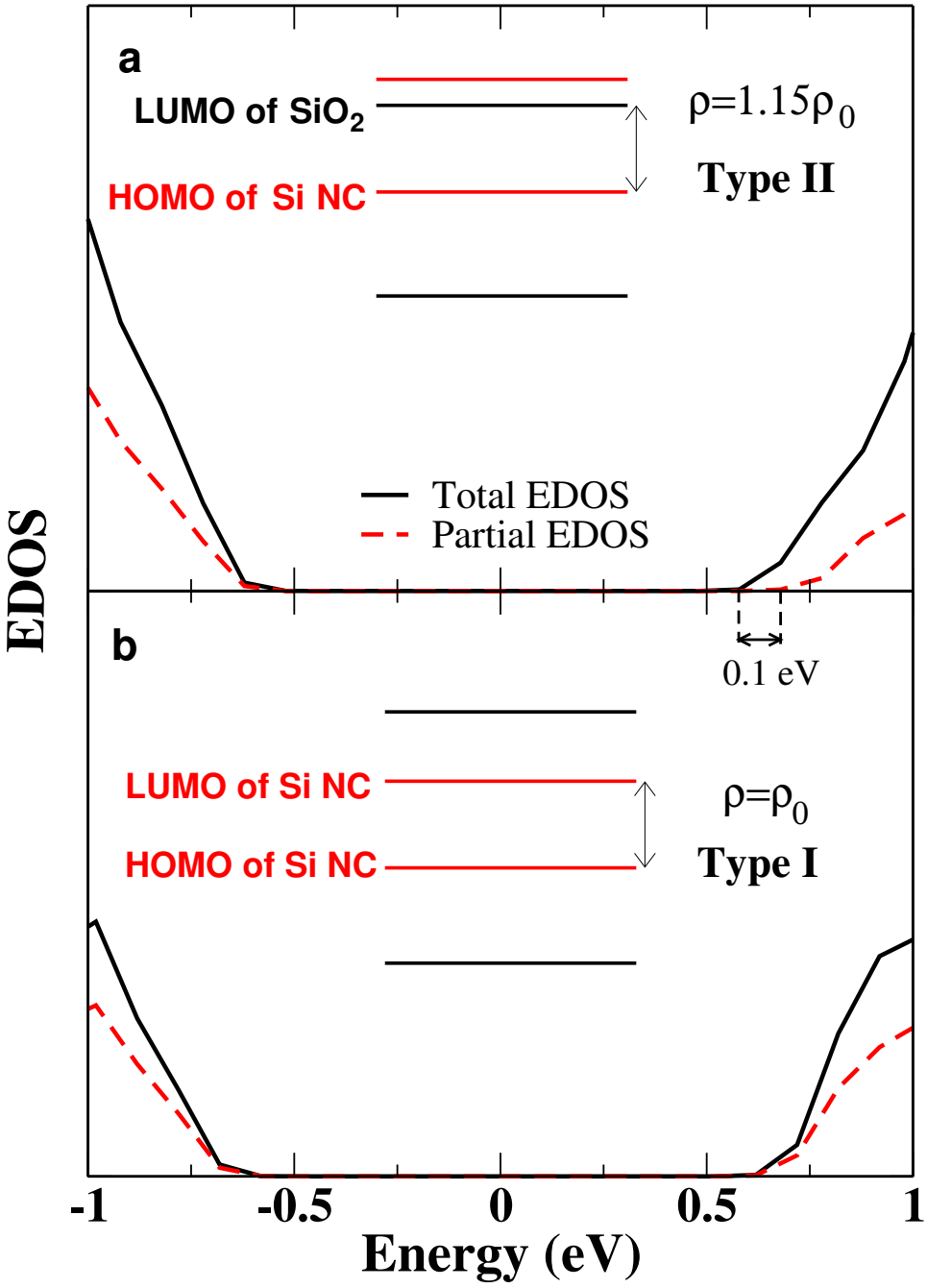

FIG. 4. The calculated EDOS near the band gap of a 1.5 nm Si NC embedded in (**a**) high density matrix ($\rho = 1.15\rho_0$) and, (**b**) equilibrium density (ρ_0) matrix. The inserts show the schematic representations of the resulting heterojunctions. The black solid and red dashed lines represent the total EDOS of the composite and the projected EDOS onto the Si NC, respectively. The energy level of the mid-gap is set at zero. The LUMO of the Si NC is about 0.1 eV above the CB minimum of the matrix.

TABLE I. Compuational models of Si nanocrystals embedded in an amorphous SiO_2 matrix

Model	#1	#2	#3	#4	#5
Diameter of Si NC (nm)	1.3	1.5	1.9	1.3	1.5
Number of Si atoms in NC	61	102	217	69	89
Average density ρ_0 (g/cm^{-3})	2.21	2.24	2.24	2.26	2.49
HOMO-LUMO Gap (eV)	1.76	1.63 [a]	1.43	1.73	1.60[b]

[a] 1.60 eV for LDA

[b] 1.49 eV for LDA